

Reaction mechanism and kinetics of boron removal from molten silicon via CaO-SiO₂-CaCl₂ slag treatment and ammonia injection

Chen, Hui; Yuan, Xizhi; Morita, Kazuki; Zhong, Yanjun; Ma, Xiaodong; Chen, Zhiyuan; Wang, Ye

DOI

[10.1007/s11663-019-01639-4](https://doi.org/10.1007/s11663-019-01639-4)

Publication date

2019

Document Version

Final published version

Published in

Metallurgical and Materials Transactions B: Process Metallurgy and Materials Processing Science

Citation (APA)

Chen, H., Yuan, X., Morita, K., Zhong, Y., Ma, X., Chen, Z., & Wang, Y. (2019). Reaction mechanism and kinetics of boron removal from molten silicon via CaO-SiO₂-CaCl₂ slag treatment and ammonia injection. *Metallurgical and Materials Transactions B: Process Metallurgy and Materials Processing Science*, 50(5), 2088-2094. <https://doi.org/10.1007/s11663-019-01639-4>

Important note

To cite this publication, please use the final published version (if applicable).
Please check the document version above.

Copyright

Other than for strictly personal use, it is not permitted to download, forward or distribute the text or part of it, without the consent of the author(s) and/or copyright holder(s), unless the work is under an open content license such as Creative Commons.

Takedown policy

Please contact us and provide details if you believe this document breaches copyrights.
We will remove access to the work immediately and investigate your claim.



Communication

Reaction Mechanism and Kinetics of Boron Removal from Molten Silicon *via* CaO-SiO₂-CaCl₂ Slag Treatment and Ammonia Injection

HUI CHEN, XIZHI YUAN, KAZUKI MORITA, YANJUN ZHONG, XIAODONG MA, ZHIYUAN CHEN, and YE WANG

To improve the boron-removal efficiency of metallurgical-grade silicon by increasing the reaction rate, a combined method with the 30 mol pct CaO-23.3 mol pct SiO₂-46.7 mol pct CaCl₂ slag treatment and ammonia injection at 1723 K to 1823 K was proposed. For 1 hour and at 1823 K, the maximum removal efficiency of boron was 98 pct, and the final boron concentration in silicon decreased to 1.5 ppmw by the present method without the introduction of the iron catalyst. A kinetic model was also established to clarify the reaction mechanism and rate-limiting steps of this complicated boron-removal process. In this model, the rate-limiting step is the mass transfer of boron oxide at the interface between the slag and silicon phase.

<https://doi.org/10.1007/s11663-019-01639-4>

© The Minerals, Metals & Materials Society and ASM International 2019

Energy crises and environmental degradation have led to higher demands on the installed capacity of solar cells, which has increased from 7.7 GW in 2009 to 72.9 GW in 2017.^[1] Silicon-based solar cells accounted for more than 94 pct of the global photovoltaic (PV) market in 2017 owing to their low cost, high-photoelectric conversion efficiency, and stability.^[2] Because of the fast growth of the PV market,^[3] the main source of

solar-grade silicon (SOG-Si) today is the non-prime electronic-grade silicon (EG-Si), which is produced by conventional processes (*e.g.*, modified Siemens process and fluidized bed process) with more economical parameters (*e.g.*, higher production efficiency and lower purity grades).^[4] However, an extra doping process is required to achieve high-photoelectric conversion efficiency of the solar modules; this reduces the purity and increases the manufacturing cost.^[5] In the metallurgical route, which has immense potential for the large-scale production of SOG-Si from metallurgical-grade silicon (MG-Si) directly, boron (B) removal is most difficult.^[6]

In the CaO-MgO-Al₂O₃-SiO₂ slag treatment process, the distribution coefficient of B does not change much when changing the slag composition,^[7] while the addition of Al₂O₃ decreases the reaction rate because of the increased viscosity.^[8] The CaCl₂-CaO-SiO₂ slag system has shown to be potentially beneficial for B removal due to both oxidization and chlorination.^[9] However, the final B concentration in Si does not yet meet the industrial demand.^[10] A method using the iron catalyst and ammonia (NH₃) was recently reported, where NH₃ displays a better selectivity for B.^[11] In this work, a method for B removal from molten Si *via* CaO-SiO₂-CaCl₂ slag treatment and NH₃ injection was proposed to achieve a higher removal rate, and a kinetic model was presented to clarify the reaction mechanism of the volatile slag-NH₃ gas-Si system. Similar to other models for their target impurities,^[12,13] this model can predict the change in the B concentration in Si with time to some extent.

The cross-sectional configuration of the shaft furnace system in our experiments is detailed in Figure 1. The samples were heated in a graphite crucible with MoSi₂ heating elements. All reactions were performed with high-purity anhydrous chemicals. The slag, with an optical basicity of 0.66, showed the highest removal efficiency of B^[14]; hence, the chosen composition of the slag was 30 mol pct CaO-23.3 mol pct SiO₂-46.7 mol pct CaCl₂.

Under an Ar atmosphere (flow rate: 0.5 standard liter per minute (SLM)), 10 g of Si (m_m) containing 75 ppmw of B and 20 g of slag (m_s) were added to the graphite crucible and then heated at 1723 K, 1773 K, and 1823 K. After the slag and Si were melted, the temperature was maintained at the same heating temperature; subsequently, NH₃ gas (> 99.9 vol pct) dehydrated by lime powders was blown to the molten slag through a magnesia tube (4 mm I. D., 5 mm O. D.) for 15 to 60 minutes. The flow rate and pressure of the NH₃ gas at the inlet were 0.1 SLM and 1 atm, respectively. After the experiments, the samples were quenched to room temperature, and the B concentrations in the slag and Si were measured by the Inductively Coupled Plasma Optical Emission Spectrometry (Optima 8000, PerkinElmer). The above procedure was repeated three times.

HUI CHEN is with the School of Chemical Engineering, Sichuan University, Chengdu 610065, Sichuan, P.R. China and also with the Department of Materials Engineering, The University of Tokyo, Tokyo 113-8654, Japan. XIZHI YUAN, YANJUN ZHONG, and YE WANG are with the School of Chemical Engineering, Sichuan University. Contact e-mail: wangye@scu.edu.cn KAZUKI MORITA is with the Department of Materials Engineering, The University of Tokyo. XIAODONG MA is with the School of Chemical Engineering, The University of Queensland, Brisbane, QLD 4072, Australia. ZHIYUAN CHEN is with the Department of Materials Science and Engineering, Delft University of Technology, 2628 CD, Delft, The Netherlands.

Manuscript submitted May 5, 2019.

Article published online July 12, 2019.

The B concentrations in the slag and Si, and the maximal removal efficiency at 1723 K to 1823 K are listed in Table I. The B concentration decreased to 1.5 ppmw at 1823 K within 1 hour, and the highest removal efficiency obtained was 98 pct. Compared to Chen *et al.*'s results in Table I,^[11] the current data were obtained with a shorter treatment period without the iron catalyst.

The B removal process in this model is illustrated in Figure 2(a). The B removal process was assumed to be divided into 6 steps: (1) mass transfer in molten Si, (2) reaction at the interface (Si/slag), (3) mass transfer from the interface (Si/slag) to the interface (NH₃-slag) and the interface (slag/gas), (4) reaction at the interface (NH₃-slag), (5) reaction at the interface (slag/gas), and (6) evaporation from the interface (slag/gas) to the gas phase. At high temperatures, the B removal process is controlled by mass transfer, and interfacial reactions can reach local equilibrium at the phase boundaries. The B concentration in the bulk phase is homogeneous because

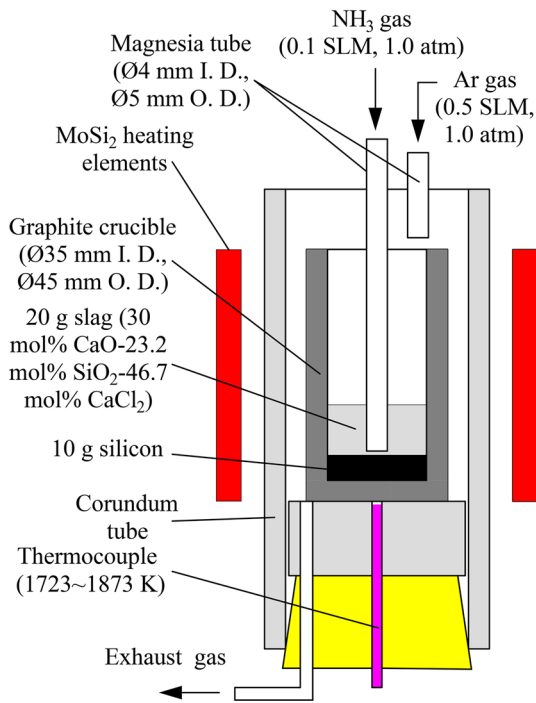
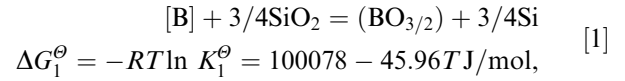


Fig. 1—Cross-sectional configuration of experimental setup.

of the fluid movement due to NH₃ blowing. Generally, the mass transfer in the gas phase (step (6)) does not need to be considered because of the high-diffusion rate of BOC1.^[15] Concentration gradients only exist at phase boundaries, and when this removal process is governed by the double-film theory, only steps (2), (4), and (5) need to be considered. The symbols used in this model are listed in the NOMENCLATURE.

Considering step (2), which is detailed in Figure 2(e), the reaction, as shown in Eq. [1], can be determined by the mass transfer of reactants and products.^[16]



where [] represents a component in Si and () a component in the slag.

The diffusion rates of [B], (BO_{3/2}), and (SiO₂) are shown in Eqs. [2] through [4].

$$J_{[B]} = k_{[B]}(c_{[B]} - c_{[B],i}), \quad [2]$$

$$J_{(BO_{3/2})}^{m-s} = k_{(BO_{3/2}),i}(c_{(BO_{3/2})} - c_{(BO_{3/2}),i}), \quad [3]$$

$$J_{SiO_2} = k_{SiO_2}(c_{SiO_2} - c_{SiO_2,i}). \quad [4]$$

Due to the local equilibrium at the reaction boundary, the equilibrium constant can be expressed as

$$K_1^\ominus = \frac{\gamma_{(BO_{3/2})} c_{(BO_{3/2})} a_{[Si],i}^{3/4}}{a_{SiO_2,i}^{3/4} \gamma_{[B]} c_{[B],i}}. \quad [5]$$

In most interfacial reactions at high temperatures, the chemical reactions are not the rate-limiting step^[17]; therefore, when reaching the local steady-state, the rate of the overall interfacial reaction can be represented as

$$J_{[B]} = -J_{(BO_{3/2})}^{m-s} = J_{SiO_2}. \quad [6]$$

$a_{[Si],i}$ is assumed to be 1 due to the reference state of the pure substance. The value of $a_{SiO_2,i}$ is 0.14,^[16] according to the basicity of the slag (the amount of CaCl₂ has generally no effect on the basicity of the slag). Hence, the reaction rate of [B] at the interface (Si/slag) can be expressed as follows:

Table I. Experimental Data at Different Temperatures in This Work and Chen *et al.*'s Results

| Time (min) | 0 | 15 | 30 | 45 | 60 | Maximal Removal Efficiency (Pct) | |
|---|------------|------------|------------|------------|------------|----------------------------------|---|
| | | | | | | This Work | Chen <i>et al.</i> 's Results (More Than 6 h) ^[11] |
| Boron Concentration in Silicon (ppmw) | | | | | | | |
| 1723 K | 75 ± 0.2 | 59.2 ± 3.4 | 34.7 ± 4.0 | 26.2 ± 8.2 | 13.6 ± 1.4 | 82 | 81 (134 → 25 ppmw) |
| 1773 K | 75 ± 0.2 | 42.5 ± 3.1 | 5.9 ± 1.0 | 4.1 ± 0.5 | 3.5 ± 0.5 | 95 | 96 (120 → 4.8 ppmw) |
| 1823 K | 75 ± 0.2 | 26.3 ± 8.0 | 8.1 ± 2.7 | 2.9 ± 0.3 | 1.5 ± 0.5 | 98 | 99 (120 → 0.89 ppmw) |
| Boron Concentration in the Slag (ppmw) | | | | | | | |
| 1723 K | 11.0 ± 1.0 | 15.6 ± 3.3 | 24.1 ± 4.0 | 19.2 ± 0.8 | 14.9 ± 3.0 | — | — |
| 1773 K | 11.0 ± 1.0 | 10.8 ± 2.0 | 22.3 ± 5.4 | 14.1 ± 0.4 | 13.3 ± 1.4 | — | — |
| 1823 K | 11.0 ± 1.0 | 9.0 ± 3.2 | 11.2 ± 6.5 | 4.2 ± 1.0 | 2.3 ± 0.7 | — | — |

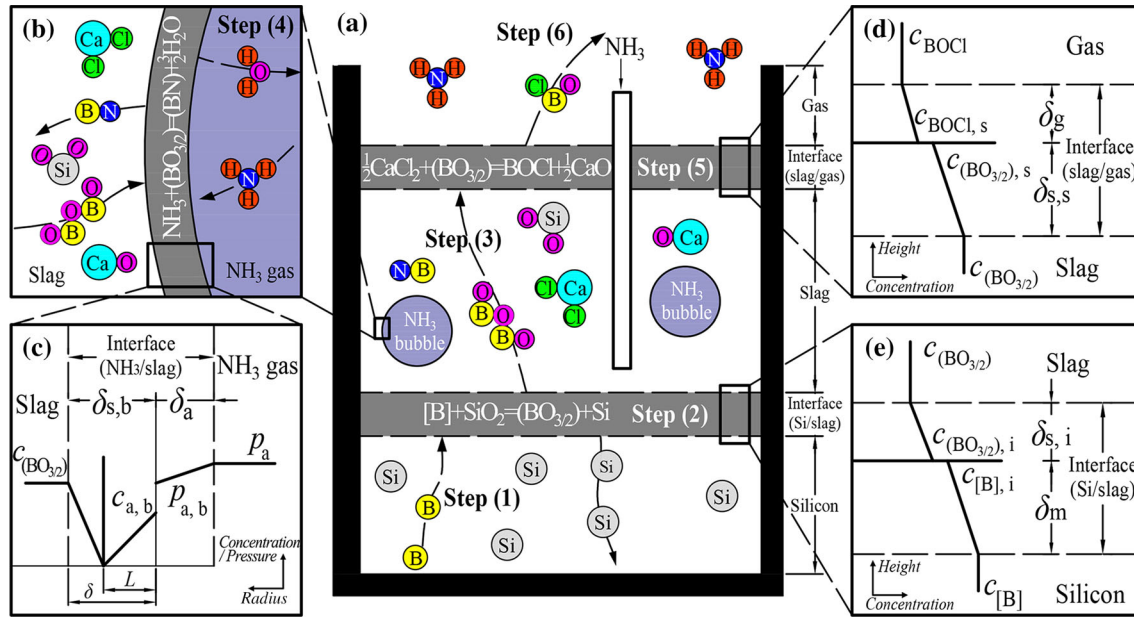
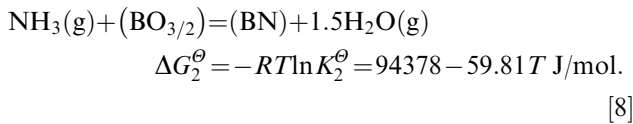


Fig. 2—Reaction mechanism of boron removal using CaCl₂-CaO-SiO₂ slag and NH₃ gas. (a) Overall reaction process and the scale of the reactor. (b) Partial details of the reaction at the interface (NH₃-slag). Reaction kinetics at (c) interface (NH₃-slag), (d) interface (slag/gas), and (e) interface (Si/slag).

$$\left\{ \begin{array}{l} J_{[B]} = -\frac{V_m d c_{[B]}}{S_i d t} = \frac{\frac{\gamma_{[B]}}{\gamma_{(BO_{3/2})}} K_1^\ominus c_{[B]} - c_{(BO_{3/2})}}{\frac{\gamma_{[B]}}{\gamma_{(BO_{3/2})}} K_1^\ominus / k_{[B]} + 1/k_{(BO_{3/2}),i}} \\ J_{m-s}^{(BO_{3/2})} = \frac{V_s d c_{(BO_{3/2})}}{S_i d t} = \frac{\frac{\gamma_{[B]}}{\gamma_{(BO_{3/2})}} K_1^\ominus c_{[B]} - c_{(BO_{3/2})}}{\frac{\gamma_{[B]}}{\gamma_{(BO_{3/2})}} K_1^\ominus / k_{[B]} + 1/k_{(BO_{3/2}),i}} \end{array} \right. \quad [7]$$

As for step (4), shown in Figure 2(c), the reaction(s) between the NH₃ gas bubbles and slag must be very complicated, because the chemical decomposition of NH₃ inevitably occurs at high temperatures. There are many compounds containing B, N, O, and H in this system, such as B₃H₆N₃, B₂H₆, HBO, and BN,^[18,19] and the most thermodynamically favored reaction, calculated by the HSC 6.0 software, is expressed as



There are some assumptions to simplify this step. BN is difficult to decompose, and is concentrated in the slag phase. At the reaction boundary, the reaction is completed instantly; therefore, NH₃ and BO_{3/2} appear on each side of the interface (NH₃/slag). This is a mass transfer process coupling with the reaction in Eq. [8], and the reaction rate is expressed as Eq. [9] when this

reaction is assumed to be a second-order reaction. In addition, H₂O formed in this step will go through the boundary layer and then into the nearest bubbles.

$$\left\{ \begin{array}{l} \frac{d c_a}{d t} = D_a \frac{d^2 c_a}{d r^2} - k_r \gamma_a c_a \gamma_{(BO_{3/2})} c_{(BO_{3/2})} \\ \frac{d c_{(BO_{3/2})}}{d t} = D_{(BO_{3/2})} \frac{d^2 c_{(BO_{3/2})}}{d r^2} - k_r \gamma_a c_a \gamma_{(BO_{3/2})} c_{(BO_{3/2})} \end{array} \right. \quad [9]$$

Ignoring the mass transfer resistance in the NH₃ bubbles and following Henry's law, the boundary conditions are as follows:

$$0 < r < L, \quad c_{(BO_{3/2})} = 0, \quad [10]$$

$$L < r < \delta, \quad c_a = 0, \quad [11]$$

$$r = 0, \quad c_a = c_{a,b} = p_a/H, \quad [12]$$

$$r = \delta, \quad c_{(BO_{3/2})} = c_{(BO_{3/2}),b}, \quad [13]$$

and

$$r = L, \quad c_a = c_{(BO_{3/2})} = 0, \quad D_{(BO_{3/2})} \frac{d c_{(BO_{3/2})}}{d r} + D_a \frac{d c_a}{d r} = 0. \quad [14]$$

Solving Eq. [9], the solution is as follows:

$$\begin{cases} c_a = c_{a,b} \left(1 - \left(1 + \frac{D_{(\text{BO}_{3/2})} c_{(\text{BO}_{3/2}),b}}{D_a c_{a,b}} \right) \frac{r}{\delta} \right) \\ c_{(\text{BO}_{3/2})} = c_{(\text{BO}_{3/2}),b} \left(1 - \left(1 + \frac{D_a c_{a,i}}{D_{(\text{BO}_{3/2})} c_{(\text{BO}_{3/2}),b}} \right) \frac{(\delta-r)}{\delta} \right) \end{cases} \quad [15]$$

Assuming that

$$k_{(\text{BO}_{3/2}),b} = \frac{D_{(\text{BO}_{3/2})}}{\delta_{s,b}}, \quad [16]$$

the consumption rate of $\text{BO}_{3/2}$ is obtained as

$$-r_{(\text{BO}_{3/2})} = -\frac{1}{4\pi r^2} \frac{dn_{(\text{BO}_{3/2})}}{dt} = -\frac{c_{(\text{BO}_{3/2})} + \frac{D_{\text{NH}_3}}{D_{(\text{BO}_{3/2})}} \frac{p_{\text{NH}_3}}{H}}{1/k_{(\text{BO}_{3/2}),b}} \quad [17]$$

The Reynolds number calculated by Eq. [18] is less than 500, which shows that the size of the bubbles is determined by buoyancy and surface tension.

$$\text{Re}_0 = \frac{u_0 d_0 \rho_s}{\mu_s} = 10.5 < 500, \quad [18]$$

where $u_0 = 0.1$ SLM, $d_0 = 4 \times 10^{-3}$ m, $\rho_s = 2800 - 0.45T$ kg/m³, [15] and $\mu_s = 0.02$ Pa s.

The bubble diameter d_b is independent of the flow rate of NH_3 and can be estimated by Eq. [19]. [20]

$$d_b = \left[\frac{6d_0\sigma}{g(\rho_s - \rho_g)} \right]^{1/3} = 4.98 \times 10^{-3} \text{m}, \quad [19]$$

where $\sigma = 0.2$ N/m, [21] and $\rho_g = 0.126$ kg/m³.

Then, when $d_b > 2$ mm and $2 < \text{Re} < 400$, the bubbles are considered to be spherical, and the average rising rate of the bubbles can be calculated by the empirical formula in Eq. [20]. [22]

$$u_b = \frac{d_b^2 g}{12} (\rho_s - \rho_g) \quad [20]$$

The number of bubbles existing simultaneously in the slag phase is given by Eq. [21].

$$n = \frac{u_0 d_0 h_s}{\pi d_b^3 u_b / 6}, \quad [21]$$

where $h_s = m_s / (\rho_s \cdot S_i)$.

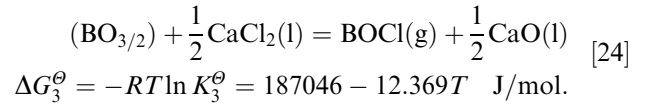
The total reaction rate of step (4) is shown by Eq. [22].

$$J_{(\text{BO}_{3/2})}^{s-g} = -\frac{1}{4\pi r^2 n} \frac{dn_{(\text{BO}_{3/2})}}{dt} = -\frac{c_{(\text{BO}_{3/2})} + \frac{D_{\text{NH}_3}}{D_{(\text{BO}_{3/2})}} \frac{p_{\text{NH}_3}}{H}}{1/k_{(\text{BO}_{3/2}),b}} \quad [22]$$

When $1 < \text{Re} < 100$, the mass transfer coefficient $k_{(\text{BO}_{3/2}),b}$ can be estimated by Eq. [23].

$$\begin{aligned} Sh &= \frac{k_{(\text{BO}_{3/2}),b} d_b}{D_{(\text{BO}_{3/2})}} = 2 + 0.55 \text{Re}^{0.55} Sc^{0.33} \\ &= 2 + 0.55 \left(\frac{u_0 d_0 \rho_s}{\mu_s} \right)^{0.55} \left(\frac{\mu_s}{\rho_s D_{(\text{BO}_{3/2})}} \right)^{0.33} \end{aligned} \quad [23]$$

In step (5), as shown in Figure 2(d), $\text{BO}_{3/2}$ is transferred through the interface (slag/gas), where the chlorination of $\text{BO}_{3/2}$ occurs, as shown in Eq. [24].



Because of the higher evaporation rate of CaCl_2 , [10] the mass transfer of BOCl can be assumed to be so fast that $c_{(\text{BO}_{3/2}),s} = c_{\text{BOCl},s} = c_{\text{BOCl}} = 0$. According to the definition of mass flux, this step can be expressed as

$$J_{(\text{BO}_{3/2})}^{s-g} = -\frac{V_s dc_{(\text{BO}_{3/2})}}{S_s dt} = \frac{(c_{(\text{BO}_{3/2})} - c_{(\text{BO}_{3/2}),s})}{1/k_{(\text{BO}_{3/2}),s}} \quad [25]$$

The area of the surface increases when bubbles burst, as shown in Figure 3; therefore, S_s can be calculated by Eq. [26].

$$S_s = S_i + n\pi r^2 = S_i + n\pi d_b^2 / 4 \quad [26]$$

Upon integrating Eqs. [7], [22], [25], and [26], Eq. [27] is derived as

$$\begin{cases} \frac{dc_{[\text{B}]}}{dt} = -\frac{\frac{7[\text{B}]}{(\text{BO}_{3/2})} K_1^\ominus c_{[\text{B}]}^{-c_{(\text{BO}_{3/2})}} S_i}{\frac{7[\text{B}]}{(\text{BO}_{3/2})} K_1^\ominus / k_{[\text{B}]} + 1/k_{(\text{BO}_{3/2}),s}} \frac{S_i}{V_m} \\ \frac{dc_{(\text{BO}_{3/2})}}{dt} = \frac{\frac{7[\text{B}]}{(\text{BO}_{3/2})} K_1^\ominus c_{[\text{B}]}^{-c_{(\text{BO}_{3/2})}} S_i}{\frac{7[\text{B}]}{(\text{BO}_{3/2})} K_1^\ominus / k_{[\text{B}]} + 1/k_{(\text{BO}_{3/2}),s}} \frac{S_i}{V_s} - \frac{c_{(\text{BO}_{3/2})} + \frac{D_{\text{NH}_3}}{D_{(\text{BO}_{3/2})}} \frac{p_{\text{NH}_3}}{H}}{k_{(\text{BO}_{3/2}),b}} \frac{4\pi r^2 n}{V_s} - \frac{c_{(\text{BO}_{3/2})}}{1/k_{(\text{BO}_{3/2}),s}} \frac{S_s}{V_s} \end{cases} \quad [27]$$

When the initial boundary conditions are $t = 0$, $c_{[\text{B}]} = c_{[\text{B}],0}$, and $c_{(\text{BO}_{3/2})} = c_{(\text{BO}_{3/2}),0}$, and assuming that

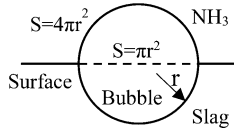


Fig. 3—Change in the area of the surface.

$$\alpha = \frac{S_i}{K_1^\ominus/k_{[B]} + 1/k_{(BO_{3/2}),i}} \left(\frac{\gamma_{[B]}}{\gamma_{(BO_{3/2})}} \frac{K_1^\ominus}{V_m} + \frac{1}{V_s} \right) + \frac{1}{V_s} \left(\frac{S_s}{1/k_{(BO_{3/2}),s}} + \frac{4\pi r^2 n}{1/k_{(BO_{3/2}),b}} \right),$$

$$\beta = \left[\frac{S_i}{K/k_{[B]} + 1/k_{(BO_{3/2}),i}} \left(\frac{\gamma_{[B]}}{\gamma_{(BO_{3/2})}} \frac{K_1^\ominus}{V_m} + \frac{1}{V_s} \right) + \frac{1}{V_s} \left(\frac{S_s}{1/k_{(BO_{3/2}),s}} + \frac{4\pi r^2 n}{1/k_{(BO_{3/2}),b}} \right) \right]^2 - \frac{4K_1^\ominus S_i}{V_m V_s (K/k_{[B]} + 1/k_{(BO_{3/2}),s})} \frac{\gamma_{[B]}}{\gamma_{(BO_{3/2})}} \times \left(\frac{S_s}{1/k_{(BO_{3/2}),s}} + \frac{4\pi r^2 n}{1/k_{(BO_{3/2}),b}} \right),$$

$$r_1 = -\frac{\alpha - \sqrt{\beta}}{2}, \quad r_2 = -\frac{\alpha + \sqrt{\beta}}{2},$$

$$a = \frac{V_m \left(K_1^\ominus \frac{\gamma_{[B]}}{\gamma_{(BO_{3/2})}} / k_{[B]} + 1/k_{(BO_{3/2}),i} \right)}{S_i},$$

$$b = \frac{\frac{D_{NH_3}}{D_{(BO_{3/2})}} \frac{p_{NH_3}}{H} \frac{4\pi r^2 n}{1/k_{(BO_{3/2}),b}}}{\left(\frac{S_s}{1/k_{(BO_{3/2}),s}} + \frac{4\pi r^2 n}{1/k_{(BO_{3/2}),b}} \right) K_1^\ominus \frac{\gamma_{[B]}}{\gamma_{(BO_{3/2})}}},$$

$$C_1 = \frac{c_{(BO_{3/2}),0} - \left(ar_2 + K_1^\ominus \frac{\gamma_{[B]}}{\gamma_{(BO_{3/2})}} \right) c_{[B],0} - abr_2}{a(r_1 - r_2)},$$

and

$$C_2 = -\frac{c_{(BO_{3/2}),0} - \left(ar_1 + K_1^\ominus \frac{\gamma_{[B]}}{\gamma_{(BO_{3/2})}} \right) c_{[B],0} - abr_1}{a(r_1 - r_2)}.$$

the solution of Eq. [27] and the curve of BN concentration are as follows:

$$\begin{cases} c_{[B]} = C_1 \exp(r_1 t) + C_2 \exp(r_2 t) - b \\ c_{(BO_{3/2})} = C_1 \left(ar_1 + K_1^\ominus \frac{\gamma_{[B]}}{\gamma_{(BO_{3/2})}} \right) \exp(r_1 t) \\ + C_2 \left(ar_2 + K_1^\ominus \frac{\gamma_{[B]}}{\gamma_{(BO_{3/2})}} \right) \exp(r_2 t) - K_1^\ominus \frac{\gamma_{[B]}}{\gamma_{(BO_{3/2})}} b \end{cases}, \quad [28]$$

and

$$c_{BN} = \frac{C_1 \left(ar_1 + K_1^\ominus \frac{\gamma_{[B]}}{\gamma_{(BO_{3/2})}} \right)}{\frac{V_s}{4\pi r^2 n k_{(BO_{3/2}),b}} r_1} \exp(r_1 t) + \frac{C_2 \left(ar_2 + K_1^\ominus \frac{\gamma_{[B]}}{\gamma_{(BO_{3/2})}} \right)}{\frac{V_s}{4\pi r^2 n k_{(BO_{3/2}),b}} r_2} \exp(r_2 t) + b K_1^\ominus \frac{\gamma_{[B]}}{\gamma_{(BO_{3/2})}} \frac{S_s}{1/k_{(BO_{3/2}),s}} t - \left[\frac{C_1 \left(ar_1 + K_1^\ominus \frac{\gamma_{[B]}}{\gamma_{(BO_{3/2})}} \right)}{\frac{V_s}{4\pi r^2 n k_{(BO_{3/2}),b}} r_1} + \frac{C_2 \left(ar_2 + K_1^\ominus \frac{\gamma_{[B]}}{\gamma_{(BO_{3/2})}} \right)}{\frac{V_s}{4\pi r^2 n k_{(BO_{3/2}),b}} r_2} \right], \quad [29]$$

where $c_{[B],0} = 75$ ppmw, $c_{(BO_{3/2}),0} = 11$ ppmw, $S_i = 7.07 \times 10^{-4} \text{ m}^2$, $m_m = 10 \text{ g}$, $m_s = 20 \text{ g}$, $\gamma_{(BO_{3/2})} = 0.23$,^[23] $\log(\gamma_{[B]}) = -11,100/T + 5.82$,^[23] $\rho_m = 2580 - 0.159(T - 1687) - 1.15 \times 10^{-4}(T - 1687)^2 \text{ kg/m}^3$,^[24] $V_m = m_m/\rho_m$, $V_s = m_s/\rho_s$, $p_{NH_3} = 101,325 \text{ Pa}$, and $H = 1.62 \times 10^{-10} \text{ Pa m}^3/\text{mol}$. $k_{[B]}$ is $2.40 \times 10^{-4} \text{ m/s}$ (1823 K), $1.70 \times 10^{-5} \text{ m/s}$ (1773 K),^[25] and $6.85 \times 10^{-6} \text{ m/s}$ (1723 K).^[26] $k_{(BO_{3/2}),i}$ is $1.91 \times 10^{-5} \text{ m/s}$ (1823 K),^[15] $1.8 \times 10^{-5} \text{ m/s}$ (1773 K), and $6.2 \times 10^{-6} \text{ m/s}$ (1723 K).^[27] $k_{(BO_{3/2}),s}$ is $2.50 \times 10^{-5} \text{ m/s}$ (1823 K),^[15] $6.4 \times 10^{-6} \text{ m/s}$ (1773 K), and $1.01 \times 10^{-6} \text{ m/s}$ (1723 K).^[25] $D_{BO_{3/2}}$ equals $8.46 \times 10^{-9} \text{ m}^2/\text{s}$ (1723 K), $1.05 \times 10^{-8} \text{ m}^2/\text{s}$ (1773 K), and $1.29 \times 10^{-8} \text{ m}^2/\text{s}$ (1823 K).^[10]

The B concentrations in Si and slag were calculated by Eq. [28]. The theoretical curves of Si essentially agree with the experimental data, as shown in Figure 4. In fact, the B concentrations in the slag are difficult to detect accurately, which may explain why they are not in good accordance with the present model.

As for Eq. [8], the equilibrium constant is represented as Eq. [30], which can explain why there is a peak in every curve for the B concentration in the slag.

$$K_2 = \frac{p_{H_2O}^{1.5} \gamma_{(BN)} c_{(BN)}}{Pa \gamma_{(BO_{3/2})} c_{(BO_{3/2})}} = \frac{[1.5(p^\ominus - p_a)]^{1.5}}{Pa} \frac{\gamma_{(BN)} c_{(BN)}}{\gamma_{(BO_{3/2})} c_{(BO_{3/2})}} \quad [30]$$

At the early stage, the BN concentrations of slag are quite low; therefore, the reaction rate of Eq. [8] is so high that the evaporation of $BO_{3/2}$ at the interface (slag/gas) is the rate-limiting step. BN concentrations in the slag increase with reaction time, thereby increasing the reaction rate of the interfacial reaction at the interface (Si/slag). Thus, the B concentrations in the slag increase rapidly. In the subsequent stage, BN cannot be separated from the slag, which causes a

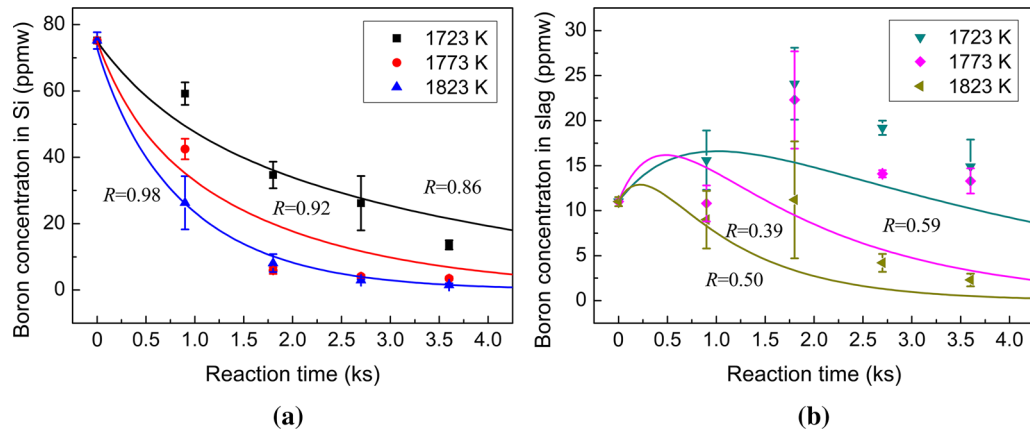


Fig. 4—Experimental data (points) on B concentrations in Si (a) and slag (b) compared with the theoretical curves of the present model.

slowdown in the nitridation of $\text{BO}_{3/2}$. Hence, the formation of BN is the rate-limiting step in this stage. This is the reason why there is a decrease after the maximum B concentration in the slag. However, this is only a conjecture because it is difficult to determine the BN concentrations in the slag.

In Chen *et al.*'s experiments,^[11] NH_3 was used to generate the ammonia atmosphere, and there was no slag between the ammonia gas and silicon. However, in the present experiments, the NH_3 gas was blown into the slag phase above the Si phase. The ammonia reacted with boron oxide instead of boron, which may explain why the catalyst iron is not necessary in the experiments.

Compared to Chen *et al.*'s results by the method using the iron catalyst and ammonia in Table I, the present data are acceptable because the reaction time is very short. Additionally, in this method, the iron catalyst is not required, which is one of the most significant merits of the process.

In conclusion, a method to remove boron from silicon via CaCl_2 - CaO - SiO_2 slag treatment and ammonia injection was carried out at 1723 K to 1823 K. The highest removal efficiency was up to 98 pct at 1823 K for 1 hour. A kinetic model was established to clarify the complicated reaction mechanism and the mass transfer in the removal of boron from molten silicon. In this model, the boron oxidation (step (2)) is the rate-limiting step. This model, which agrees well with the experimental data, can be used to predict the limits of boron removal. For example, if all data listed in the NOMENCLATURE are provided, the curve representing the B concentration in Si with time can be obtained from this model.

NOMENCLATURE

| | |
|-----------------------|--|
| T | Kelvin temperature (K) |
| ρ_m | The density of silicon (kg/m^3) |
| ρ_g | The density of ammonia (kg/m^3) |
| $c_{[\text{B}]}$ | The B concentration in Si (mol/m^3) |
| c_{SiO_2} | The SiO_2 concentration in the slag (mol/m^3) |
| c_a | The NH_3 concentration in the slag (mol/m^3) |
| $\gamma_{[\text{B}]}$ | The activity coefficient of B |

| | |
|------------------------------|--|
| $c_{[\text{B}], 0}$ | Initial B concentration in Si (mol/m^3) |
| $k_{[\text{B}]}$ | Mass transfer coefficient of B at the interface (Si/slag) (m/s) |
| $k_{(\text{BO}_{3/2}),s}$ | Mass transfer coefficient of $\text{BO}_{3/2}$ at the interface (slag/gas) (m/s) |
| $k_{(\text{BO}_{3/2}),b}$ | Mass transfer coefficient of $\text{BO}_{3/2}$ at the interface (NH_3 /slag) (m/s) |
| p_a | The pressure of bubbles (Pa) |
| μ_s | The viscosity of the slag (Pa s) |
| u_0 | The flow rate of NH_3 in the corundum tube (m/s) |
| σ | Surface tension between NH_3 gas and slag (N/m) |
| g | Gravitational constant (N/kg) |
| Sh | Sherwood number |
| $a_{[\text{Si}]}$ | The activity of Si |
| V_m | The volume of Si (m^3) |
| V_s | The volume of the slag (m^3) |
| $D_{(\text{BO}_{3/2})}$ | Diffusion coefficient of $\text{BO}_{3/2}$ in the slag (m^2/s) |
| H | Henry's constant ($\text{Pa m}^3/\text{mol}$) |
| R | Ideal gas constant ($\text{J}/(\text{K}\cdot\text{mol})$) |
| ρ_s | The density of the slag (kg/m^3) |
| $c_{(\text{BO}_{3/2})}$ | The B concentration in the slag (mol/m^3) |
| c_{BOCl} | BOCl concentration in gas (mol/m^3) |
| $\gamma_{(\text{BO}_{3/2})}$ | The activity coefficient of $\text{BO}_{3/2}$ |
| γ_a | The activity coefficient of NH_3 |
| $c_{(\text{BO}_{3/2}),0}$ | Initial $\text{BO}_{3/2}$ concentration in the slag (mol/m^3) |
| r | The average radius of bubbles (m) |
| k_{SiO_2} | Mass transfer coefficient of SiO_2 at the interface (Si/slag) (m/s) |
| $k_{(\text{BO}_{3/2}),i}$ | Mass transfer coefficient of $\text{BO}_{3/2}$ at the interface (Si/slag) (m/s) |
| k_r | The constant for Eq. [9] (m/s) |
| d_0 | The diameter of ammonia gas tube (m) |
| d_b | The average diameter of bubbles (m) |
| u_b | The rising rate of bubbles in the slag (m/s) |
| δ | The thickness of the boundary layer (m) |
| h_s | The height of the slag (m) |
| Sc | Schmidt number |
| a_{SiO_2} | The activity of SiO_2 |
| S_i | The area of the interface (Si/slag) (m^2) |
| S_s | The area of the interface (slag/gas) (m^2) |

D_a Diffusion coefficient of NH_3 in the slag (m^2/s)
 t Reaction time (s)

This work was supported by the NSFC Project (No. 51604176), and the Chengdu Science and Technology Benefiting Project (No. 2016-HM01-00399-SF). We thank for Mr. Amit Patel (The University of Tokyo) for his linguistic assistance during the preparation of this manuscript.

REFERENCES

1. L.P. Bloomberg Finance: Q4 2016 Global PV Market outlook, 2016, pp. 1–3.
2. Fraunhofer ISE: *Photovoltaics Report*, Fraunhofer ISE, Freiburg, 2017, pp. 19–20.
3. Y. Wang and K. Morita: *Metall. Mater. Trans. B*, 2016, vol. 47B, pp. 1542–47.
4. L. Huang, H. Lai, C. Gan, H. Xiong, P. Xing, and X. Luo: *Sep. Purif. Technol.*, 2016, vol. 170, pp. 408–16.
5. H. Morito, M. Uchikoshi, and H. Yamane: *Sep. Purif. Technol.*, 2013, vol. 118, pp. 723–26.
6. H.C. Theuerer: *JOM*, 1956, vol. 8 (10), pp. 1316–19.
7. L.K. Jakobsson and M. Tangstad: *Metall. Mater. Trans. B*, 2018, vol. 49B, pp. 1699–1708.
8. M.S. Islam and M.A. Rhamdhani: *Metall. Mater. Trans. B*, 2018, vol. 49B, pp. 3171–85.
9. Y. Wang, X. Ma, and K. Morita: *Metall. Mater. Trans. B*, 2014, vol. 45B, pp. 334–37.
10. H. Chen, Y. Wang, W. Zheng, Q. Li, X. Yuan, and K. Morita: *Metall. and Mater. Trans. B*, 2017, vol. 48B, pp. 3219–27.
11. Z. Chen and K. Morita: *Metall. Mater. Trans. E*, 2016, vol. 3E, pp. 228–30.
12. M. Vadon, Ø. Sortland, I. Nuta, C. Chatillon, M. Tansgtad, G. Chichignoud, and Y. Delannoy: *Metall. Mater. Trans. B*, 2018, vol. 49B, pp. 1288–1301.
13. J.E. Olsen, I.T. Kero, T.A. Engh, and G. Tranell: *Metall. Mater. Trans. B*, 2017, vol. 48B, pp. 870–77.
14. G. Qian, Z. Wang, X. Gong, and L. Sun: *Metall. Mater. Trans. B*, 2017, vol. 48B, pp. 3239–50.
15. Y. Wang and K. Morita: *J. Sustain. Metall.*, 2015, vol. 1, pp. 26–33.
16. L.A.V. Teixeira, Y. Tokuda, T. Yoko, and K. Morita: *ISIJ Int.*, 2009, vol. 49, pp. 777–82.
17. W. Jiang, W. Yu, H. Qin, Y. Xue, C. Li, and X. Lv: *Int. J. Hydrogen Energy*, 2019, vol. 44 (26), pp. 13502–08.
18. Z. Xia, J. Wu, W. Ma, Y. Lei, K. Wei, and Y. Dai: *Sep. Purif. Technol.*, 2017, vol. 187, pp. 25–33.
19. C. Lu, L. Huang, H. Lai, M. Fang, W. Ma, P. Xing, L. Zhang, J. Li, and X. Luo: *Sep. Sci. Technol.*, 2015, vol. 50 (17), pp. 2759–66.
20. I. Leibson, E.G. Holcomb, A.G. Cacosso, and J.J. Jacmic: *AIChE J.*, 1956, vol. 2, pp. 300–06.
21. J.R. Grace, T. Wairegi, and T.H. Nguyen: *Trans. Inst. Chem. Eng.*, 1976, vol. 54, pp. 167–73.
22. Y. Marcus: *Thermochim. Acta*, 2013, vol. 571, pp. 77–81.
23. L.A.V. Teixeira and K. Morita: *ISIJ Int.*, 2009, vol. 49, pp. 783–87.
24. W.K. Rhim and K. Ohsaka: *J. Cryst. Growth*, 2000, vol. 208, pp. 313–21.
25. L. Zhang: Ph.D. dissertation, Dalian university of Technology, 2013.
26. L. Zhang, Y. Tan, J. Li, Y. Liu, and D. Wang: *Mater. Sci. Semicond. Proc.*, 2013, vol. 16, pp. 1645–49.
27. F. Wang, J. Wu, W. Ma, Y. Lei, K. Wei, and B. Yang: *J. Chem. Thermodyn.*, 2018, vol. 118, pp. 215–24.

Publisher's Note Springer Nature remains neutral with regard to jurisdictional claims in published maps and institutional affiliations.